An Analysis of Nonlinear Relationship between the MJO and ENSO

Youmin TANG

Environmental Science and Engineering, University of Northern British Columbia, Prince George, Canada

and

Bin YU

Climate Research Division, Environment Canada, Toronto, Canada

(*Manuscript received 20 August 2007, in final form 22 July 2008*)

Abstract

Using the Hilbert Singular Value Decomposition (HSVD) and the Nonlinear Canonical Correlation Analysis (NLCCA), we analyzed the statistical relationship of MJO (Madden-Julian Oscillation) and ENSO (El Niño and Southern Oscillation). It was found that while a linear analysis produced no significant relationship between MJO and ENSO, a low-order nonlinear analysis based on the quadratic function of HSVD led to statistically significant lagged correlations. When their nonlinear relationship was further extracted by the NLCCA, stronger correlation was obtained, with the maximum correlation coefficient appearing while the MJO signals preceding the ENSO signals by around 2 months and 5–6 months respectively. The time lags producing the maximum correlation are respectively consistent with the characteristic time of MJO influencing ENSO dominated by two physical processes: the equatorial Kelvin waves and air-sea feedback. Corresponding to the two different physical processes, ENSO shows different features of development. In the former scenario, the westerly winds in the western Pacific excite the equatorial Kelvin waves which propagate eastward and deepen the thermocline in the eastern Pacific, resulting in the sea surface warming at the far eastern Pacific near the coast. In the latter scenario, the westerly anomalies in the western Pacific precede the development of El Niño through bringing surface warm water into the central and eastern Pacific, thus the sea surface warming occurs across the whole eastern Pacific ocean.

1. Introduction

Study of the interaction of MJO and ENSO has long been of interest, not only because they are dominant atmospheric and oceanic modes of variability on intraseasonal and interannual timescales respectively, but because they both have significant impact on global climate anomalies. In addition, the study may have important implications for climate prediction, especially for the prediction of ENSO. Many studies show that MJO could be seen as an integral component of the tropical coupled climate system and appears to interact with and affect the evolution of the ENSO cycle (e.g., Nitta and Motoki 1987; Lau et al. 1989; McPhaden 1999; Zhang 2005). For example, Kessler and Kleeman (2000) found that an idealized "MJO forcing" can lead to changes in the thermal structure of the oceanic mixed layer which could in turn impact ENSO. Zhang and Gottschalck (2002) showed that during ENSO warm events, amplitudes of sea surface temperature anomalies (SSTA) in the eastern Pacific can be affected by MJO through its seasonal activity of Kelvin wave forcing, with a significant leading time of 6–10 months between the MJO activity over the western Pacific and ENSO. With the sensitivity

Corresponding author: Youmin Tang, Environmental Science and Engineering, University of Northern British Columbia, 3333 University Way, Prince George, BC, Canada, V2N 4Z9.
E-mail: ytang@unbc.ca

experiments of intermediate and hybrid coupled models, Zavala-Garay et al. (2003; 2005) and Moore et al.(2006) also found that "MJO-forcing" can explain a large fraction of the interannual variability in an asymptotically stable version of the model. In their experiments, "MJO-forcing" was usually defined with a relatively large-scale structure in space and random red noise in time. Seiki and Takayabu (2007) found that westerly wind bursts, closely related to MJO convection, have significant lagged correlations with ENSO by 1–10 months leads. The time lags of correlation vary from different regions of the Indian and the Pacific Ocean.

While the observation and modeling showed the link between MJO and ENSO, statistically significant relationship between them has not been well identified. For example, Slingo et al. (1999) derived an MJO index based on the first two principal components (PCs) of the zonal mean of band-passed 200-mb zonal wind and found that there is no statistically significant correlation between the MJO index and ENSO. Hendon et al. (1999) also reported little relationship between MJO and ENSO. Kessler (2001) found that the first two major EOF (empirical orthogonal function) modes of intraseasonal outgoing long-wave radiation and zonal wind are unrelated to ENSO, though MJO activity shifts eastward in conjunction with ENSO. Thus the relationship between MJO and ENSO is still a topic of debate. The central question here is whether the link between MJO and ENSO as noted above is random in nature, thereby no statistically significant relationship existing, or nonlinear that linear statistical techniques fail to identify.

One widely used strategy in studying the relationship of MJO-ENSO is to apply the EOF to datasets (e.g., lower-layer zonal wind, precipitation or outgoing long-wave radiation) to extract MJO modes, and then to correlate them with ENSO. This is a linear approach, which can not identify any nonlinear relationship. The MJO and ENSO are dominant atmospheric and oceanic variability with very different time scales, thus their relationship, if existed, is most probably nonlinear. In fact, recently Hendon et al. (2007) and McPhaden et al. (2006) found that the relationship of MJO and ENSO varies with the season, and identified a good linear relationship using MJO index in late boreal spring and SSTA Nino3.4 index in the subsequent autumn/winter. They also found that using data from all months biases the fact of seasonal dependence of MJO-ENSO connection. Such a high seasonal dependence of MJO-ENSO connection strongly suggests a general nonlinear relationship between them. In addition, they used the amplitude function of PC-defined MJO index, a quadratic function, to compute the MJO-ENSO relationship. Therefore the linear correlation identified could be statistically viewed as equivalent to a nonlinear relationship of a PC-defined MJO index with ENSO (also see Section 5). The nonlinear statistical techniques have not been applied to analyze the relationship of MJO-ENSO, simply because appropriately nonlinear methods, such as the neural network approach (e.g., Tang et al. 2001; Teng et al. 2004), were introduced and applied to atmospheric and oceanic sciences only in recent years.

The other issue is relevant to the domain of dataset. Usually the data used in defining MJO covers a global domain of longitude. While a global range of longitude was considered here to address the fundamental large-scale features of MJO activity, the defined MJO index also takes weight on the Indian Ocean that is not highly relevant to ENSO (also see Section 5). As argued by Kessler (2001), it is not the zonal average or total MJO activity that is related to ENSO, but a specific element of the MJO activity over the Pacific where sea surface temperature (SST) is very sensitive to equatorial oceanic processes. In addition, ENSO is primarily a local coupling mode in the tropical Pacific Ocean (Tang, 2002).

In this study we use nonlinear statistical techniques and focus on the tropical Pacific Ocean to explore the effect of MJO activity on ENSO. This paper is structured as follows: Section 2 briefly describes the data and analysis technique. Section 3 discusses the relationship of MJO-ENSO using a defined MJO index which characterizes the basic nonlinearity of MJO. Section 4 further presents a statistical relationship between MJO and ENSO using NLCCA, followed by discussion and conclusions in Section 5.

2. The data and analysis technique

To characterize the state of MJO and ENSO, daily surface zonal winds from the National Centers for Environmental Prediction-National Center for Atmospheric Research (NCEP-NCAR) reanalysis (Kalnay et al. 1996) and monthly SST from Reynolds SST analyses (Reynolds and Smith 1994) were used respectively. The data for the period 1981 to 2000 was analyzed due to the relatively poor quality of the zonal wind data before 1980 (e.g., Wu and

Xie 2003). Also the introduction of satellite data in 1979 may bring some effects on the analysis. On the other hand, the daily dataset of 20 years contains 7300 samples in time, which should be sufficient to derive robust statistical results.

Daily values of the SST were obtained by interpolation using a linear scheme as in Zavala-Garay et al. (2005). The data domain of zonal wind was the whole equatorial strip of the Pacific Ocean from 120°E to 70°W and 15°N to 15°S, which contained most of the convective variability of the Pacific MJO; for SST, we concentrated on the tropical-subtropical Pacific Ocean (20°S to 20°N, 120°E to 70°W), which embodied most of the ENSO SST anomalies.

The climatology annual cycle for each calendar day was computed, and then subtracted from the raw data for each dataset. To obtain the intraseasonal variability, a fifth-order Butterworth bandpass filter with a 30 to 90 d period was used to filter the zonal wind anomaly data.

2.1 Hilbert Singular Value Decomposition (HSVD)

A standard signal detection technique, the HSVD, was first used to extract the PCs of the MJO variability. Compared with conventional SVD or EOF which only depict stationary modes, HSVD is capable of detecting propagating waves enabling it to better characterize MJO properties. In HSVD the covariance is computed using a complex matrix, therefore HSVD is also called complex EOF (CEOF). The complex matrix $\mathbf{U}$ should be constructed with the real data matrix $\mathbf{M}$ using a Hilbert Transforms, i.e., $\mathbf{U} = \mathbf{M} + \tilde{\mathbf{M}}$, where $\tilde{\mathbf{M}}$ is the imaginary part corresponding with the real part $\mathbf{M}$. According to the theory of Hilbert Transforms,

$$\tilde{\mathbf{M}}(t) = \sum_{l=-L}^{L} \mathbf{M}(t-l)h(l) \tag{1}$$

where

$$h(l) = \begin{cases} \dfrac{2}{l\pi}\sin^2(l\pi/2) & \text{if } l \neq 0; \\ 0, & \text{if } l = 0. \end{cases}$$

Ideally $L = \infty$ in (1),but in this study $L = 7$ as in Barnett (1983).

HSVD produces complex eigenvectors and complex time series, which can characterize such important propagation features as amplitude and phase for the analyzed variable. Naturally, the amplitude $\mathbf{B}$ and phase θ in a complex domain is defined as below

$$\mathbf{R} = \mathbf{B} * \mathbf{B}^*; \theta = \arctan\left[\frac{\mathrm{Im}\,\mathbf{B}}{\mathrm{Re}\,\mathbf{B}}\right] \tag{2}$$

where $\mathbf{B}^*$ is conjugate of $\mathbf{B}$. When $\mathbf{B}$ is an eigenvector, the $\mathbf{R}$ and θ represent spatial features of propagating waves, whereas when $\mathbf{B}$ is a time series, they characterize the temporal evolution of the propagating waves. More information on HSVD can be found in Barnett (1983) and Zavala-Garay et al. (2005).

2.2 Nonlinear Canonical Correlation Analysis (NLCCA)

In conventional Canonical Correlation Analysis (CCA), the canonical variates $\mathbf{u}$ and $\mathbf{v}$ are a linear combination of the input variables,

$$\mathbf{u} = \mathbf{a} \cdot \mathbf{x} \quad \mathbf{v} = \mathbf{b} \cdot \mathbf{y} \tag{3}$$

where the weight vectors $\mathbf{a}$ and $\mathbf{b}$ are chosen subject to the following conditions: (i) corr($\mathbf{u}$, $\mathbf{v}$), the correlation between $\mathbf{u}$ and $\mathbf{v}$, is to be maximum. (ii) var($\mathbf{u}$) and var($\mathbf{v}$), the variances of $\mathbf{u}$ and $\mathbf{v}$, are to be unity.

In NLCCA, the same procedure is followed as in CCA, except that the linear mappings in (3) are replaced by nonlinear mapping functions using NNs, i.e.,

$$u = \mathbf{NN}^x(\mathbf{x}) \quad v = \mathbf{NN}^y(\mathbf{y}) \tag{4}$$

Where $\mathbf{NN}^x$ and $\mathbf{NN}^y$ are the nonlinear mappings from the vector spaces of data $\mathbf{x}$ and $\mathbf{y}$ to the new vector space of u and v. After obtaining u and v, we can return to the original data space by inverse maps $\mathbf{NN}^u$ and $\mathbf{NN}^v$, i.e.,

$$\hat{\mathbf{x}} = \mathbf{NN}^u(u) \quad \hat{\mathbf{y}} = \mathbf{NN}^v(v) \tag{5}$$

An important issue in NLCCA is how to derive the nonlinear functions (operators) $\mathbf{NN}$ from the inherent structure of the dataset. This has been implemented by neural networks (Kramer 1991), since they can simulate any nonlinear continuous functions (Cybenko 1989). Figure 1 shows the architecture of a common network (e.g., $\mathbf{NN}^x$), which places between the input and output variables (also called 'neurons'), a layer of 'hidden neurons'. The value of the j-th hidden neuron is

$$y_j = \tanh\left(\sum_i w_{ij} x_i + b_j\right), \quad j = 1,\ldots,m. \tag{6}$$

where x_i is the i-th input, m is the number of hidden neurons, characterizing the extent of the nonlinearity, w_{ij} the weight parameters and b_j the bias parameters. The output neuron is given by

$$u = \sum_j^m \tilde{w}_j y_j + \tilde{b}. \tag{7}$$

To obtain a network **NN** is actually to determine the parameters w_{ij}, $\tilde{w}_j$, b_j and $\tilde{b}$ according to data sets. This is usually implemented by a constraint optimization. Therefore, $\mathbf{NN}^x$ and $\mathbf{NN}^y$ can be obtained by optimization subject to the conditions (i) and (ii), whereas $\mathbf{NN}^u$ and $\mathbf{NN}^v$ can be extracted by respectively minimizing the cost functions J1 and J2:

$$\mathrm{J1} = (\mathbf{x} - \hat{\mathbf{x}})^{tr}(\mathbf{x} - \hat{\mathbf{x}}), \quad \mathrm{J2} = (\mathbf{y} - \hat{\mathbf{y}})^{tr}(\mathbf{y} - \hat{\mathbf{y}}) \tag{8}$$

where *tr* denotes the transpose.

In contrast to CCA, as the mapping functions **NN**s are nonlinear, there is not a single spatial pattern associated with an NLCCA mode. The approximation $\hat{\mathbf{x}}$ and $\hat{\mathbf{y}}$, however, correspond to a sequence of different patterns that can be visualized cinematographically. For linear CCA, the approximation $\mathbf{a}^{tr}\mathbf{u}$ and $\mathbf{b}^{tr}\mathbf{v}$ (Eq. 3) produce a standing wave pattern as the PCs (**u** and **v**) vary, whereas with NLCCA the spatial pattern generally changes as the nonlinear PCs vary. We will use the $\hat{\mathbf{x}}$ and $\hat{\mathbf{y}}$ corresponding to a few u and v values to explore the changing spatial structures of the NLCCA modes. A detailed algorithm of NLCCA was introduced in Hsieh (2001), which first proposed the method. Some applications of NLCCA in meteorology/oceanography can be found in Wu and Hsieh (2002) and Tang and Hsieh (2002).

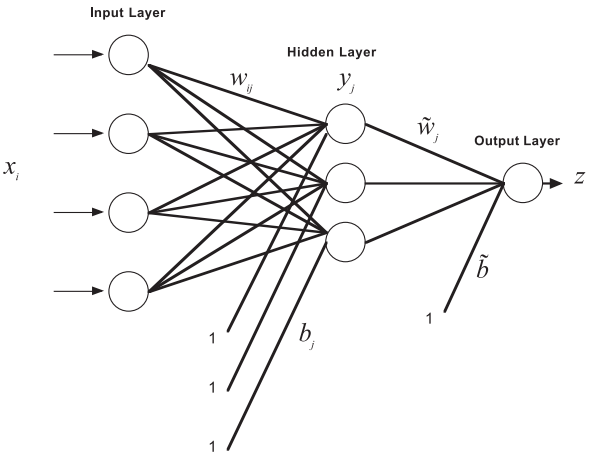

Fig. 1. An example of a neural network model, where there are four neurons in the input layer, three in the hidden layer, and one in the output layer. The parameters w_{ij} and $\tilde{w}_j$ are the weights, and b_j and $\tilde{b}$ are the biases. The parameters b_j and $\tilde{b}$ can also be regarded as the weights for constant inputs of value 1.

3. The MJO mode and the connection of MJO-ENSO

3.1 The MJO mode

Figure 2a displays the spatial amplitude function of the first HSVD mode of daily zonal winds, accounting for 37% of total variance within the domain of interest. The variance contribution by individual modes becomes rather small after the first mode (e.g., 11% and 7% for the second and the third modes respectively), and therefore we will mainly focus on the first mode in this analysis. As can be seen, the mode is primarily characterized by large magnitudes in the western and central Pacific Ocean, in particular in the off-equator

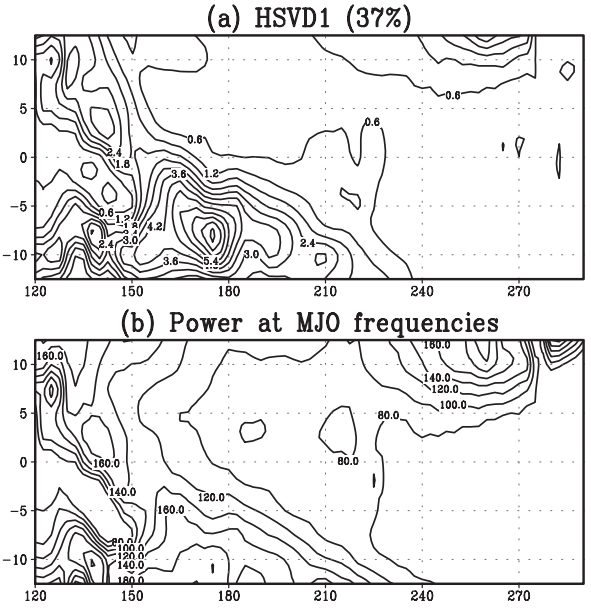

Fig. 2. (a) Spatial amplitude function of the first HSVD mode, accounting for 37% of total variance; (b) Power of the MJO frequencies (30 to 90 d^{-1}). The units are m^2 s^{-2} in both (a) and (b).

western and central Pacific ocean. Figure 2b is the spectral power of the MJO frequencies for the zonal wind, defined by the integral of the spectral power in the window with periods of 30 to 90 d. Comparing Figs. 2a and 2b shows that the structure of the first HSVD spatial amplitude function is in good agreement with the spatial distribution of the spectral power of the MJO frequencies, indicating that significant MJO signals can be characterized and represented by the first mode. The MJO signals are also apparent in the corresponding temporal amplitude function of the first mode (refereed to as HSVD PC1, not shown).

The recovered signals from the first HSVD mode, obtained by taking the real part of the product of the first HSVD complex eigenvector multiplied by the corresponding time series, show pronounced MJO properties and are characterized by an apparent disturbance propagating eastward from the western to the central and then the eastern Pacific Ocean (Fig. 3).

Based on the above analyses, we conclude that the first HSVD mode represents the spatial and temporal variability of the Pacific MJO activity well. Thus we define the first HSVD mode as the MJO mode, and its time amplitude function as the MJO index.

3.2 Relationship between MJO and ENSO

The MJO index is then employed to explore the statistical relationship between MJO and ENSO. The lagged correlation is used to examine the possible impact of MJO on ENSO. Unless otherwise indicated, the time lag is defined as the time of MJO activity leading to ENSO signals in the following discussions.

Figure 4 displays lagged correlation between the MJO and Niño3 SSTA indices. The thick line here is the correlation function with the lag time, computed using the daily MJO index and the daily Niño3 (90°W to 150°W and 5°S to 5°N) SSTA index for the period from January 1981 to December 2000. Since a 30–90 d bandpass filter was applied for generating MJO index, the interannual variability contained in the surface wind, which is highly correlated with SST interannual variability, has been removed. Thus the correlation obtained using the daily data with over 7000 samples in Fig. 4 characterizes the relationship between the intraseasonal variability of the zonal wind and the interannual variability of SST.

A critical issue for evaluating the correlations shown in Fig. 4 is the statistically significant test. Since the MJO index and Pacific SSTA are of nonzero trend and autocorrelated time series, serial correlation must be considered when a statistically significant test is performed. One common method for dealing with time series that are serially correlated is to estimate an effective sample size, and then use the standard two-tailed student's t test. However it has been found that effective sample size often could not be estimated consistently (e.g., Ebisuzaki 1997; Zwiers and von Storch 1995). An effective method to quantitatively estimate biases in correlation analysis is the Monte Carlo re-sampling test. It is a nonparametric method, and suitable for the significance test of a nonzero correlation between two time series when serial correlation is a concern. One key issue in the Monte Carlo resampling correlation test is to surrogate data sets which have the same autocorrelation as the real data. In this study, we used Ebisuzaki's method (1997) for implementing the re-sampling test. In this approach, resampling was done in the frequency domain through a Fourier transform. This procedure will not preserve the distribution of values but rather the power spectrum (periodogram), which ensures the resampled series to retain the same autocorrelation as the original series.

The thin-dashed line shown in Fig. 4 is the statistical significance criteria of correlation at a confidence level of 95%, obtained using the resampling test with 10,000 realizations for each time lag. The criteria are not sensitive to the number of realizations after the size exceeds 5000. From the Monte Carlo re-sampling test, it was found that the lagged correlation between the MJO and Niño3 SSTA indices is statistically significant for time lags of around 3-8 months, with its peak at a lag of around 5 months. In a framework of linear forcing-response, the result can be well explained by seasonal sensitivity of MJO's forcing on ENSO as reported in Zhang and Gottschalck (2002), Hendon et al. (2007), McPhaden et al. (2006) and Tang and Yu (2008). They found the significant impact of MJO activity in spring on ENSO in the subsequent autumn-winter, with a significant correlation at the time lag of 5–6 months. A possible mechanism responsible for the MJO-ENSO connection at the time lags is air-sea feedback, which is based on Bjerknes theory of trade wind (Bjerknes 1969) and recently addressed by some researchers (e.g., Hendon et al. 2007; Kessler and Kleeman 2000). The core component here is the interaction be-

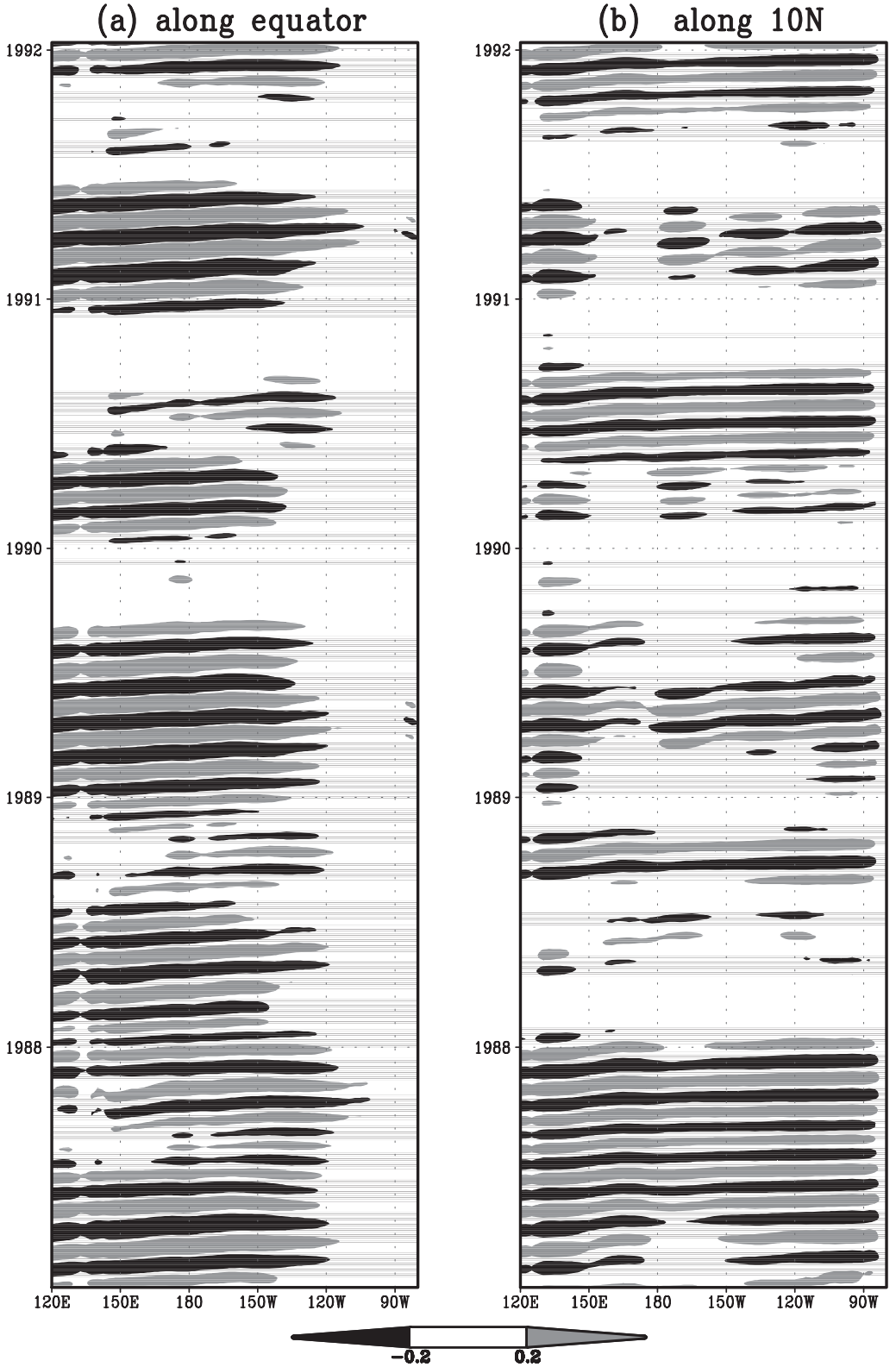

Fig. 3. Time-longitude sections of the recovered MJO signals using the first HSVD mode along (a) the equator and (b) 10°N.

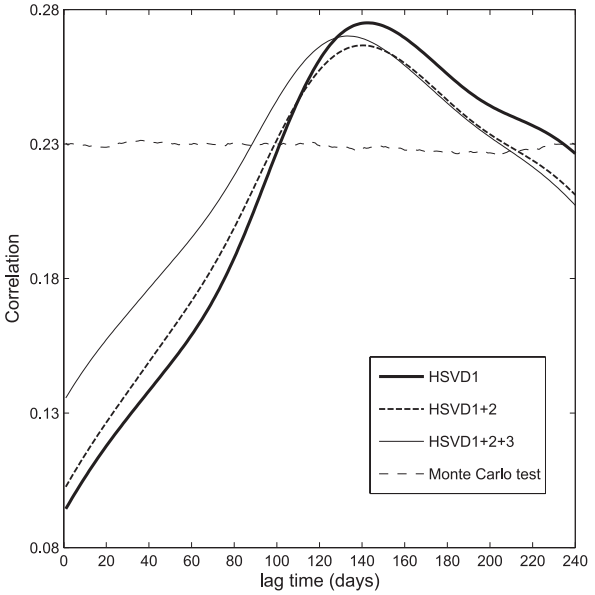

Fig. 4. Lagged correlation between the MJO and Niño3 SSTA indices (thick line). The lag is the time of MJO activity preceding ENSO variability. Dashed line is statistically significant criteria from the Monte Carlo re-sampling test at a confidence level of 95%. The MJO index including the second and third HSVD modes is also correlated with Niño3 SSTA respectively, as shown in dash-dotted line and thin line.

tween MJO-induced westerly anomalies and SST anomalies. It has been found that enhanced MJO activity often results in anomalous westerly surface winds in the western Pacific (e.g., Kessler and Kleeman 2000; Zavala-Garay et al. 2005). In general, the westerly anomalies in the western Pacific precede the development of El Niño through bringing surface warm water into the central and eastern Pacific. This process often starts in Spring. The warm water in the central and eastern Pacific enhances the SST zonal gradient on the western edge, and in turn intensifies westerly anomalies. Such a positive feedback between the westerly anomalies and SSTA in the central and eastern Pacific promotes enhanced MJO activity in the western Pacific, which then promotes enhanced surface westerlies in the western Pacific. These are highly conductive to El Niño conditions around 6–8 months later as evidenced and argued in Hendon et al. (2007).

While the above hypothesis explains MJO-ENSO relationship at the time lags of 3–8 months and the connection of MJO in the boreal spring with ENSO in autumn-winter, it is unable to interpret the connection of MJO in the summer with ENSO in the subsequent autumn-winter by a lag of around 2 months, as found in Hendon et al. (2007), McPhaden et al. (2006) and Tang and Yu (2008). The Kelvin wave theory has also been widely applied to insight the possible physical mechanism of MJO-ENSO connection (e.g., Hendon et al. 1998; McPhaden 1999; Zhang and Gottschalck 2002). However it can not explain Fig. 4, because the time lag resulting in the maximum correlation here is around 5 months, far larger than the time required for Kelvin waves across the Pacific basin. In addition, the correlation coefficients in Fig. 4 are not very compelling with the maximum value of only 0.27 although they pass Monte-Carlo significant tests.

There are two most possible reasons responsible for the aforementioned issues: (1) Only the first MJO-mode was used in the above analyses. The ignored higher modes may impact on ENSO in a shorter time scale; (2) The nonlinearity that is probably inherent to the relationship of MJO-ENSO is not represented effectively although the above analysis characterizes some nonlinear components by using the amplitude function of HSVD instead of conventional PCs as the MJO index[1]. To investigate the first issue, we redefined two MJO indices that include the second and third HSVD modes, namely the sum of the time amplitude of the first two HSVD and the first three HSVD modes. The lagged correlation between MJO and ENSO using the new indices is respectively shown in thick-dashed line and thin line in Fig. 4. As can be seen, including higher modes only lead to subtle differences of correlation. This is probably because the first three modes of HSVD share similar features as shown in Fig. 5. Thus the lack of sufficient nonlinearity in the methods used here is most probably the reason for the above results. In fact, recent progresses in identifying significant lagged correlation of MJO-ENSO are all based on using the data from some seasons. It was found that the MJO-ENSO relationship is far less significant when the data from all seasons were used (Hendon et al.

1 The amplitude function of HSVD is essentially a quadratic form of conventional PCs, and therefore its linear correlation to ENSO could reflect some nonlinear relationship of a PC-defined MJO index with ENSO.

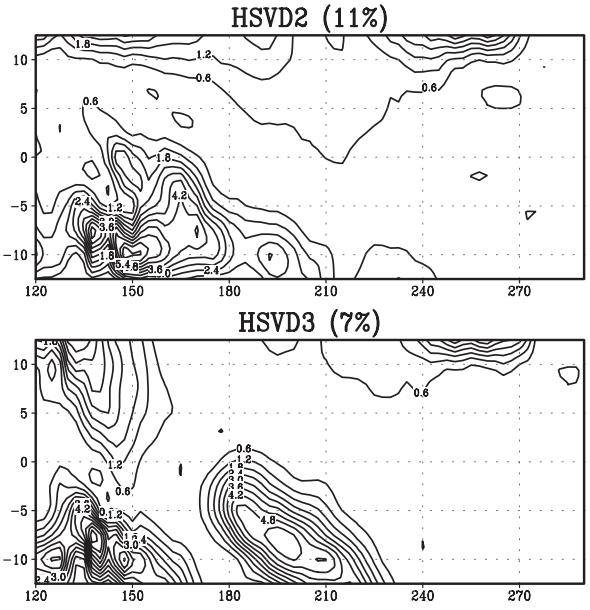

Fig. 5. Spatial amplitude function of the second and third HSVD modes.

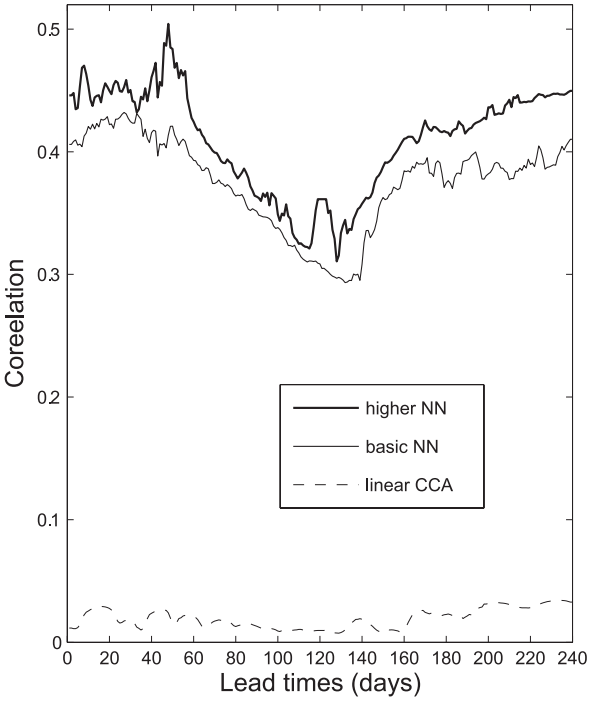

Fig. 6. Correlation coefficient between NLCCA Mode 1 of MJO and NLCCA Mode 1 of ENSO.

2007). Mathematically such a seasonal-dependent relationship could be described by a step function (nonlinear), namely good linear relationship in some seasons and no linear relationship in other seasons. Thus the overall relationship of MJO-ENSO is nonlinear in nature.

4. Nonlinear Relationship of MJO-ENSO

4.1 NLCCA analysis

In this section, we will use NLCCA introduced in Section 2 to explore the MJO-ENSO relationship. An important aspect of a **NN** is the size of the network, i.e., the number of hidden neurons m in the hidden layer for representing the nonlinear functions **NN***s*. A larger m increases the nonlinear modeling capability of the network, but could also lead to overfitted solutions (i.e., wiggly solutions which fit to the noise in the data). Based on a general principle of parsimony, the m values were varied from 2 to 5; and the weight penalty parameters (Hsieh 2001) from 0.01–0.05 for smoothing. For a given m, an ensemble of 20 **NN**s with random initial weights and bias parameters was run. Also, 20% of the data was randomly selected as test data and withheld from the training of the **NN**s. Runs where the mean square error (MSE) was larger for the test dataset than for the training dataset were rejected to avoid overfitted solutions. The **NN** with the smallest MSE was selected as the solution for the given m. The solutions from different m were further compared with respect to their MSE to get the optimal **NN** structure.

The SSTA and the filtered wind data were preprocessed by retaining only its first 6 EOF modes, which account for 90% and 56% of the total variance, respectively. The bold line shown in Fig. 6 is the correlation coefficient between u and v, the first nonlinear modes of wind and SSTA extracted from the NLCCA as defined in (4), with the number of hidden neurons of 3 and 5 for SSTA and zonal wind respectively, which lead to the best correlation of u and v in a dozen of sensitivity experiments. It should be noted that the correlation coefficient is not much sensitive to several tested numbers of hidden neurons. The thin line in Fig. 6 shows the correlation between the u and v that were extracted by a basic structure of nonlinear network, i.e., $m = 2$ for both SSTA and zonal wind. As can be seen, the correlation coefficient from a basic **NN** is in good agreement with that from a higher nonlinear network for almost all lead times, suggesting that the MJO-ENSO relationship is not

very highly nonlinear. This explains to a considerable extent why a statistically significant relationship of MJO-ENSO can also be identified using the MJO index that is defined by a quadratic function, as shown in last section. The quadratic function is the weakest nonlinear form. In contrast, the correlation from the linear CCA shown in Fig. 6 in the dashed line is very small, indicating the impact of MJO on ENSO is nonlinear, rather than linear.

The statistically significant test was performed for Fig. 6 using the Monte-Carlo re-sampling method as in last section. The resampled series were constructed for the PCs of the zonal wind and SSTA, and then the NLCCA was performed for them. This was repeated 500 times and produced a criteria given a significant level. Due to costly training process of NLCCA[2], we only preformed the Monte-Carlo re-sampling test for the time lags of 40–60 d and 200–220 d, during which there are large correlations to appear. It might be reasonable to assume that the average of the criteria values from these time lags can represent an upper level of significant test. At the significant level of 5%, the average of the criteria is 0.35 with a standard deviation of 0.02. The criteria indicates that the nonlinear relationship of MJO-ENSO is statistically significant for all lags during 0–90 d and 150–240 d, with the maximum correlation appearing at a lag of around 50 d. A very interesting feature in Fig. 6 is that small correlations during the lags of 90–150 d separate large correlations of both sides, making the relationship itself as nonlinear. The good relationship of MJO-ENSO at the lags of 0–90 d and 150–240 d explains well both the connection of MJO in the boreal spring with ENSO in autumn-winter and the connection of MJO in the summer with ENSO in the subsequent autumn-winter reported in several recent studies (Hendon et al. 2007; Tang and Yu 2008). The lag of around 50 d resulting in the maximum correlation is approximately the time required for oceanic Kelvin waves to propagate eastward across the Pacific basin, suggesting a very important role of Kelvin waves in the relationship of MJO and ENSO, as reported in previous studies (e.g., Hendon et al. 1998).

Thus Fig. 6 not only reflects the air-sea feedback mechanism responsible for MJO-ENSO connection at the lag of 5–8 months, but also identifies the Kelvin wave mechanism responsible for MJO-ENSO connection at the lag of around 2 months. The lagged correlations also show a positive impact of MJO on ENSO as evidenced by the observations – strong MJO activity occurs prior to ENSO event. The robust statistical evidence is important for our further understanding to the MJO-ENSO relationship. It should be noticed that the Kelvin wave mechanism has been used to explain MJO-ENSO connection, but the lag of 2 months, the characteristic time for Kelvin wave propagation across the basin of the Pacific ocean, has not been well identified.

Another concerned issue is whether the correlation shown in Fig. 6 is stable. To explore this, we performed several sensitivity experiments for the time lag of 49 d, i.e., performing NLCCA for this lag using several different segments of data, i.e., 80%, 70%, 60% of original data. The results show the correlations are rather stable in these experiments and their differences are subtle.

4.2 Extremes of the canonical variates

Figure 7 shows the time-longitude plot of the first NLCCA mode (referred to as NLCCA1 hereafter) at the extremes of the canonical variate v and u, i.e., during max(v) and during max(u), averaged over the equator belt of 5°S–5°N, for lag times from 0 to 240 d. Figure 7a represents the zonal wind anomalies (MJO) preceding the extreme SST anomalies (El Niño) whereas Fig. 7b shows the SST anomalies following the extreme zonal wind anomalies (MJO activity). As can be seen in Fig. 7a, strong MJO signals usually precede EL Niño events by around 20–80 d and 150–200 d, which are primarily consistent with Fig. 6. However at the two different lag periods, the zonal wind anomalies show some different features. For the period of 20–80 d lag, the strong zonal wind anomalies appear to be favorable over the western Pacific whereas for the period of 150–200 d the zonal wind anomalies tend to extend across the basin. This basin-scale westerly anomalies shown in Fig. 7a are consistent with the results in Hendon et al. (2007). Correspondingly, the SSTA patterns also show some differences in the two time lag periods as shown in Fig. 7b. The anomalous warming mainly occurs in the far eastern Pacific while MJO activity proceeding El Niño by 20–80 d, whereas the anomalous warming can extend over the whole eastern Pacific while the MJO proceeding El Niño by 140–200 d. These features are clearer in Figs. 8 and 9, the composite of NLCCA1 zonal wind when the SST anomalies

2 A Monte-Carlo test needs performing 500 (times)× 20 (ensemble size) NLCCAs

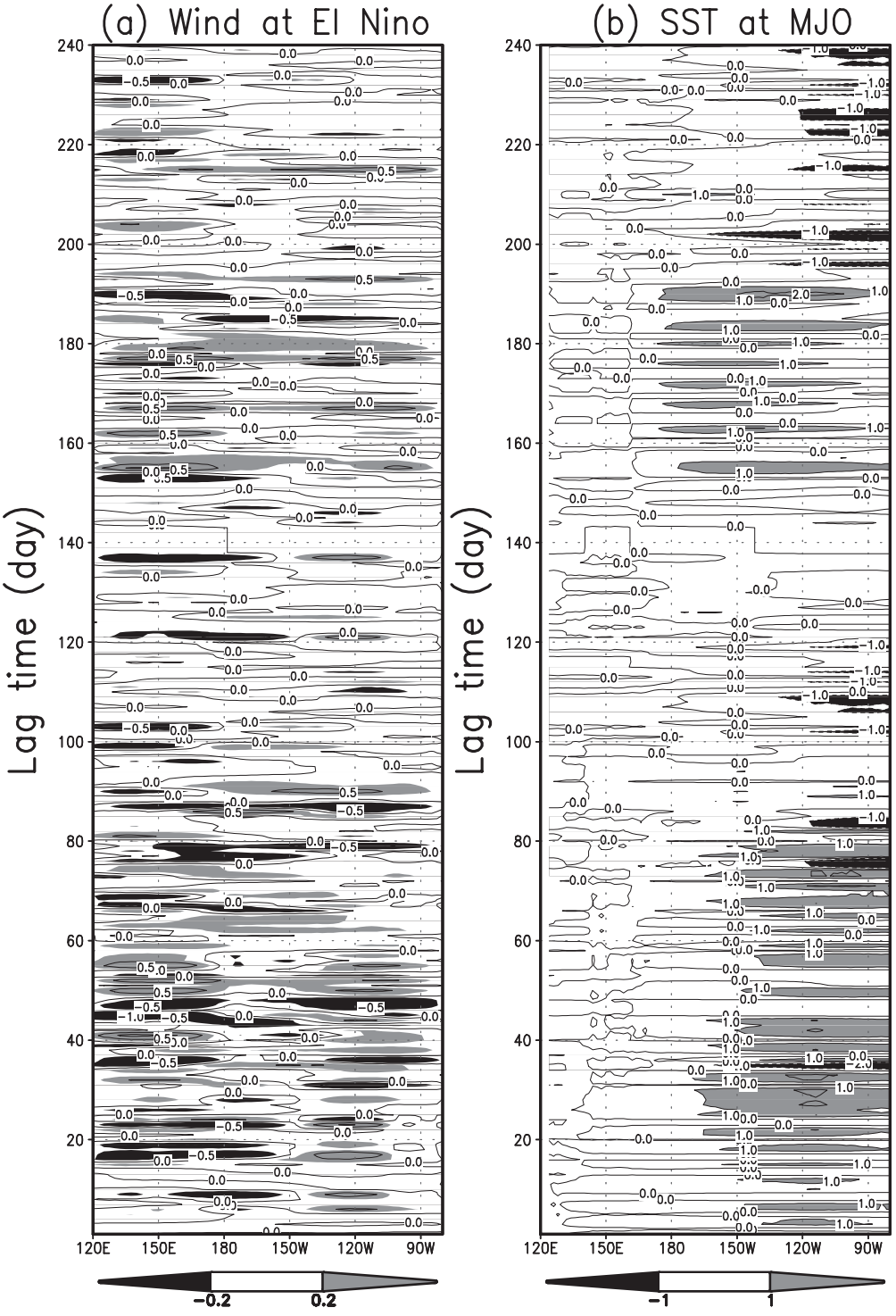

Fig. 7. (a) Time-longitude plot of zonal wind reconstructed by the first NLCCA mode, averaged over the equator belt of 5°S–5°N, when the canonical variate v (i.e., the first time series of NLCCA Model 1 of SST) is maximum, and (b) Time-longitude plot of SST anomalies reconstructed by the first NLCCA mode, averaged over the equator belt of 5°S–5°N, when the canonical variate u (i.e., the first time series of NLCCA Model 1 of Wind) is maximum. The anomalies during contour intervals are 0.5 m s^{-1} for (a) and 1.0 degree Celsius for (b).

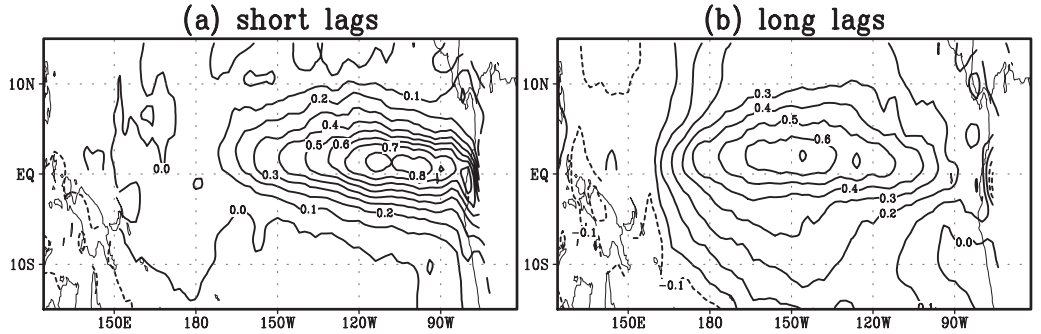

Fig. 8. Composite of SSTA reconstructed by the first NLCCA mode for the lags of (a) 50–60 d and (b) 160–170 d, when the zonal wind anomalies are maximum. The anomalies during contour intervals are 0.1 degree Celsius for (a) and (b).

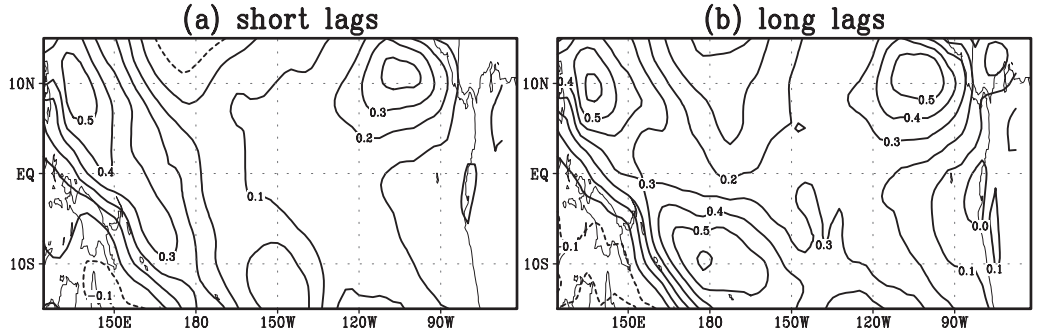

Fig. 9. Composite of zonal wind reconstructed by the first NLCCA mode for the lags of (a) 50–60 d and (b) 160–170 d, when the SST anomalies are maximum. The anomalies during contour intervals are 0.1 m s^{-1} for (a) and (b).

are maximum and the composite of NLCCA1 SSTA when the zonal wind anomalies are maximum, respectively, at the lags of 50–60 d and 160–170 d. Thus the MJO activity preceding El Niño by different lags has different impact on the SSTA pattern.

The above results may evidence two possible mechanisms of MJO-ENSO connection as discussed in the preceding section. While MJO preceding ENSO by 20–80 d, the westerly wind in the western Pacific excites the equatorial Kelvin waves which propagate eastward and deepen the thermocline in the eastern Pacific, resulting in the sea surface warming at the far eastern Pacific as shown in Fig. 8a. In this scenario, the equatorial westerly in the western Pacific (Fig. 9a) plays an important role to excite the oceanic Kelvin waves to arrive at the eastern Pacific in around 2 months. This is in good agreement with the time required for oceanic Kelvin waves to propagate eastward across the basin.

On the other hand, while MJO preceding ENSO by 150–200 d, the impact of MJO on ENSO is by the mechanism of air-sea feedback as aforementioned. In this scenario, the westerly anomalies in the western Pacific (Fig. 9b) precede the development of El Niño through bringing surface warm water into the central and eastern Pacific, thus the sea surface warming occurs across the whole region of the eastern Pacific Ocean, as shown in Fig. 8b. In addition, the strong westerly winds off the equator also weaken the equatorial upwelling, resulting in the surface warming along the equator.

The results from Figs. 7, 8 and 9 are reminiscent of the observation that enhanced MJO activity often precedes the development of El Niño (e.g., McPhaden 1999). These characteristics are inherent to underlying dynamical and physical processes causing the effect of MJO on ENSO. In an active MJO scenario, accompanying the eastward propa-

gating MJO signals, large westerly wind anomalies can directly bring warm water present in the central equatorial and eastern Pacific, which yields the warm SST and heat content (HC) anomalies in the region. This process takes about 150–200 d, and is probably a simple linear feedback between SSTA and the westerly winds, which is allowed to identify using linear methods. On the other hand, the process of MJO influencing ENSO through Kelvin waves propagation is probably nonlinear although the theory of the equatorial Kelvin waves can be described in a linear framework. The equatorial Kelvin waves do not directly change SSTA. Instead, they impact the sea surface temperature through the thermocline adjustment in the eastern Pacific, which is the most probably a nonlinear process. This might explain why the time lag yielding the maximum correlation between MJO and ENSO seems inconsistent with the time required for the Kelvin waves propagation across the basin when linear statistical methods were used in previous studies (e.g., Zhang and Gottschalck 2002). The NLCCA that can characterize the nonlinearity produces a time lag of around 2 months well consistent with the equatorial Kelvin waves theory. Thus the NLCCA results built a basic and robust statistical relationship of MJO-ENSO, and explained the relationship in a physical framework.

It is possible that MJO impacts on ENSO through a joint process of air-sea feedback and Kelvin waves. Indeed it has been reported that the Kelvin wave propagation and the surface eastward currents were observed together preceding El Niño in the previous studies (e.g., McPhaden 1999; 2004). It might be more realistic that MJO impacts ENSO by an incorporation approach of the two processes. For example, strong westerly wind anomalies bring warm water, yielding the warm SST and heat content anomalies in the central and eastern Pacific. A strong zonal HC gradient at the central equatorial Pacific weakens the upwelling there and intensifies the warm Kelvin waves propagating eastward. The warm eastward propagating Kelvin waves bring warm waters to the eastern Pacific Ocean to further intensify the anomalies. In such a joint scenario, the equatorial Kelvin wave propagation is often accompanied, even induced, by the air-sea feedback process. Thus for a short time lag, the impact of MJO on ENSO is most probably through both the air-sea feedback and the Kelvin waves propagation.

5. Discussion and Conclusions

Over the last decade considerable progress has been made in the study of MJO, including its possible impact on ENSO. Several mechanisms that are hypothetically responsible for the MJO-ENSO interaction have also been proposed among which are the air-sea feedback and the Kelvin wave theory (e.g., Zhang 2005; Hendon et al. 2007). However the relationship between MJO and ENSO is still controversial. An essential challenge is to explore whether there is a robust and statistically significant relationship between the intraseasonal MJO activity and interannual ENSO variability to support the observation that MJO activity often precedes El Niño.

There are several possible reasons to limit identifying the statistical relationship of MJO-ENSO. First, the MJO indices that are currently used to correlate with the ENSO index might not be effective metrics for this purpose. As mentioned previously, ENSO is a local coupling mode dominated by local dynamical and thermodynamical processes occurring over the equatorial Pacific Ocean. However, many MJO indices are based on datasets with a domain of both the Indian and Pacific Oceans. They could be affected by MJO activity in the Indian Ocean. Seiki and Takayabu (2007) recently studied local correlation between westerly wind bursts and ENSO and found the time lags producing significant correlation change in different regions. Second, the impact of MJO on ENSO is of nonlinearity, which is necessary for the generation of westerly wind bursts exciting the oceanic Kelvin waves (Seiki and Takayabu 2007). It has been argued that the MJO involves nonlinear signals and nonlinearly relate to ENSO and atmospheric variability (e.g., Jamet and Hsieh 2005). However, the MJO indices simply defined by leading PCs only capture the linear relationship when they are correlated with ENSO. This study aimed at the second issue while the first one was also touched. We used the Pacific zonal wind to highlight the features of the Pacific MJO activity, in particular, the amplitude function of HSVD is used to replace conventional PCs as the MJO index. The amplitude function of HSVD is essentially a quadratic form of conventional PCs, and therefore its linear correlation to ENSO is actually equivalent to a nonlinear relationship of a PC-defined MJO index with ENSO. Further we applied a recently developed nonlinear statistical technique, the nonlinear

CCA, to explore the nonlinear relationship between MJO and ENSO.

It was found that statistically significant lagged correlations exist between MJO and ENSO at two time lag period, i.e., MJO proceeding ENSO by 0–90 d and by 150–240 d. Their maximum correlations appear at a lag of around 2 and 5–6 months respectively. Such lagged correlations show a positive impact of MJO on ENSO as evidenced by observations – strong MJO activity occurs prior to El Niño whereas La Niña events often follow relatively weak MJO activity. The spatial and temporal features of the correlation variations support well the hypothesis of the connection of MJO-ENSO, which suggests that the effect of MJO activity on ENSO variability may be through MJO-excited downwelling oceanic Kelvin waves or air-sea feedback mechanism. The time lags producing the maximum correlation are consistent with the characteristic time of the physical processes responsible for MJO-ENSO connection. Such robust statistical evidence is important for our further understanding to the MJO-ENSO relationship and has important implication for ENSO prediction. Nevertheless, it should be noticed that intraseasonal forcing discussed in this study may be an important and/or necessary but not a sufficient condition for El Niño. One popular hypothesis assumes that ENSO is a linear, damped, stochastically forced system, as argued in many studies (e.g., Kleeman and Moore 1997; Penland and Sardeshmukh 1995; Chang et al. 1996; Moore and Kleeman 1999; Flügel et al. 2004; Tang et al. 2005). As one of major sources of stochastically forcing, MJO can act as an effective trigger of El Niño. Many studies show that the effects of realistic stochastic forcing applied to a hybrid coupled model or an intermediate coupled model in a regime that would otherwise be periodic are sufficient to produce irregularity generally consistent with observed ENSO signals (e.g., Blanke et al. 1997; Eckert and Latif 1997; Kleeman and Moore 1997; Moore and Kleeman 1999; Zavala-Garay et al. 2003, 2005). To make the trigger to excite and form El Niño events, some other conditions might also be required. For example, a heat content build-up along the equator is generally necessary for El Niño to develop according to recharge oscillator theory (Jin 1997a, b).

We also performed several extra analyses to further examine the relationship between MJO and ENSO: (1) We repeated all analyses performed in Section 3 with the data domain of the zonal wind extended to 40°E to 90°W. Similarly, the MJO index was defined using the amplitude function of the first HSVD (referred to as the global MJO index). Correlating the global MJO index with the tropical Pacific SSTA shows that there are no statistically significant correlations between the global MJO index and ENSO at any time lag from 0 to 240 d, as shown in Fig. 10; (2) An HSVD analysis was performed for the zonal wind of the Indian Ocean. The derived MJO index (refereed to as the Indian MJO index) is statistically uncorrelated with Niño3 SSTA, but shows a negative sign for all time lags of 0 to 240 d, as opposed to the Pacific MJO index (Fig. 10). These may shed light on the reason that previous studies that used a global MJO index did not detect a statistically significant relationship between MJO and ENSO; and (3) We repeated Section 3 using the NCEP outgoing long-wave radiation (OLR) reanalysis data for the period 1981 to 2000. The statistically significant relationship found in Section 3 also holds well using the OLR dataset, indicating that the statistical relationship between MJO and ENSO reported in this study is not data dependent.

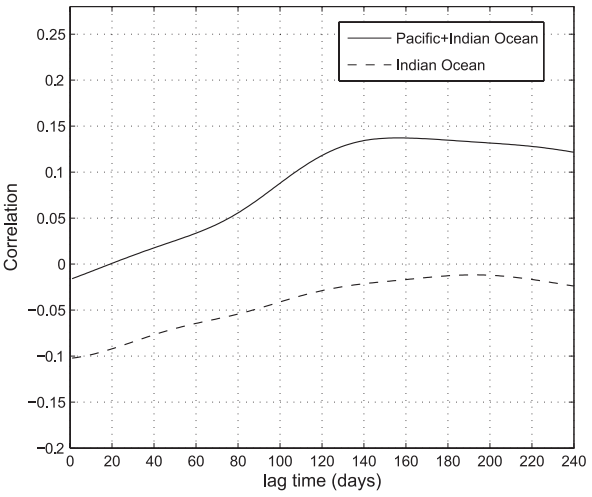

Fig. 10. Lagged correlations of Niño3 SSTA against the global MJO index (solid line), and against Indian MJO index (dashed line). The lag time is the period by which MJO activity precedes ENSO variability.

Acknowledgments

This work was supported by Canadian Foundation for Climate and Atmospheric Sciences and by

Canada Research Chair Program. YT thanks Dr. David Stephenson for his suggestion to use the Monte Carlo resampling method in this paper.

References

Barnett, T.P., 1983: Interaction of the Monsoon and Pacific Trade Wind System at Interannual Time Scales Part I: The Equatorial Zone. *Mon. Wea. Rev.*, **111**, 756–773.

Blanke, B, J.D. Neelin, and D. Gutzler, 1997: Estimating the effect of stochastic wind stress forcing on ENSO irregularity. *J. Climate*, **10**, 1473–1486.

Chang, P., L. Ji, H. Li, and M. Flügel, 1996: Chaotic Dynamics versus Stochastic Process in El Niño-Southern Oscillation in Coupled Ocean-Atmosphere Models. *Physica D*, **98**, 301–320.

Ebisuzaki, W., 1997: A Method to Estimate the Statistical Significance of a correlation when the data are serially correlated. *J. Climate*, **10**, 2147–2153.

Eckert, C. and M. Latif, 1997: Predictability of a stochastic forced hybrid coupled model of El Niño. *J. Climate*, **10**, 1488–1504.

Flügel, M., P. Chang, and M.C. Penlend, 2004: The role of stochastic forcing in modulating ENSO predictability. *J. Climate*, **17**, 3125–3140.

Hannoschock, C. and C. Frankigoul, 1985: Multivariate statistical analysis of a sea surface temperature anomaly experiment with the GISS general circulation model I. *J. Atmos. Sci.*, **42**, 1430–1450.

Hendon, H.H., C. Zhang, and J.D. Glick, 1999: Interannual variation of the Madden-Julian oscillation during austral summer. *J. Climate*, **12**, 2538–2550.

Hendon, H.H., B. Liebmann, and J.D. Glick, 1998: Oceanic Kelvin waves and the Madden-Julian Oscillation. *J. Atmos. Sci.*, **55**, 88–101.

Hendon, H.H., M. Wheeler, and C. Zhang, 2007: Seasonal dependence of the MJO-ENSO Relationship. *J. Climate*, **20**, 531–543.

Hsieh, W.W., 2001. Nonlinear canonical correlation analysis of the tropical Pacific climate variability using a neural network approach. *J. Climate*, **14**, 2528–2539.

Jamet, C. and W.W. Hsieh, 2005. The nonlinear atmospheric variability in the winter northeast Pacific associated with the Madden-Julian Oscillation. *Geophys. Res. Lett.*, **32**(13), L13820, DOI: 10.1029/2005GL023533.

Jin, F.-F., 1997a: An equatorial ocean recharge paradigm for ENSO. Part I: Conceptual model. *J. Atmos. Sci.*, **54**, 811–829.

Jin, F.-F., 1997b: An equatorial ocean recharge paradigm for ENSO. Part II: A stripped-down coupled model. *J. Atmos. Sci.*, **54**, 830–847.

Kalnay, E. and coauthors, 1996: NCEP/NCAR 40-year reanalysis project. *Bull. Amer. Meteor. Soc.*, **77**, 437–471.

Kessler, W., 2001: EOF Representations of the Madden-Julian Oscillation and its connection with ENSO. *J. Climate*, **14**, 3055–3061.

Kessler, W.S. and R. Kleeman, 2000: Rectification of the Madden-Julian Oscillation into the ENSO cycle. *J. Climate*, **13**, 3560–3575.

Kramer, M.A., 1991: Nonlinear principal component analysis using autoassociative neural networks. *AIChE Journal*, **37**, 233–243.

Kleeman, R. and A.M. Moore, 1997: A theory for the limitation of ENSO predictability due to stochastic atmospheric transients. *J. Atmos. Sci.*, **54**, 753–767.

Lau, K.M., L. Peng, T. Nakazawa, and C.H. Sui, 1989: Dynamics of super cloud clusters, westerly wind bursts, 30–60 day oscillations and ENSO – An unified view. *J. Meteor. Soc. Japan*, **67**, 205–219.

McPhaden, J.M., 1999: Genesis and evolution of the 1997–98 El Niño. *Science*, **283**, 950–954.

McPhaden, J.M., 2004: Evolution of the 2002–2003 El Niño. *Bull. Amer. Meteorol. Soc.*, **85**, 677–695.

McPhaden, J.M., X. Zhang, H. Henden, and C. Wheeler, 2006: Large scale dynamics and MJO forcing of ENSO variability. *Geophys. Res. Lett.*, **33**, LI6702, doi:10.1029/2006GL026786.

Moore, A. and R. Kleeman, 1999: Stochastic forcing of ENSO by the Intraseasonal Oscillation. *J. Climate*, **12**, 1199–1220.

Moore, A.M., J. Zavala-Garay, Y. Tang, R. Kleeman, A.T. Weaver, J. Vialard, K. Sahami, and D.L.T. Anderson, 2006: Optimal Forcing Patterns for Coupled Models of ENSO *J. Climate*, **19**, 4683–4699.

Nitta, T. and T. Motoki, 1987: Abrupt enhancement of convective activity and low-level westerly burst during the onset phase of the 1986–87 El Niño. *J. Meteor. Soc. Japan*, **65**, 497–506.

Penland, C. and P.D. Sardeshmukh, 1995: The optimal growth of tropical sea surface temperature anomalies. *J. Climate*, **8**, 1999–2024.

Reynolds, R.W. and T.M. Smith, 1994: Improved global sea surface temperature analysis using optimal interpolation. *J. Climate*, **7**, 929–948.

Seiki, A. and Y.N. Takayabu, 2007: Westerly Wind Bursts and Their Relationship with Intraseasonal Variations and ENSO. Part I: Statistics. *Mon. Wea. Rev.*, **135**, 3325–3345.

Shinoda, T. and H.H. Hendon, 2002: Rectified wind forcing and latent heat flux produced by the Madden-Julian Oscillation. *J. Climate*, **15**, 3500–3508.

Slingo, J.M., D.B. Rowell, K.R. Sperber, and F. Nortley, 1999: On the predictability of the inner annual behavior of the Madden-Julian Oscillation and its relationship with El Niño. *Quart. J. Roy. Met. Soc.*, **125**, 583–609.

Tang, Y., W.W. Hsieh, B. Tang, and K. Haines, 2001: A

neural network atmospheric model for hybrid coupled modeling. *Clim. Dyn.*, **17**, 445–455.

Tang, Y., 2002: Hybrid coupled models of the tropical Pacific – Interannual variability. *Clim. Dyn.*, **19**, 331–342.

Tang, Y. and W.W. Hsieh, 2002. Hybrid coupled models of the tropical Pacific – ENSO prediction. *Clim. Dyn.*, **19**, 343–353.

Tang, Y., R. Kleeman, and A. Moore, 2005; On the reliability of ENSO dynamical predictions. *J. Atmos. Sci.*, **62**, No. 6, 1770–1791.

Tang, Y. and B. Yu, 2008: MJO and its relationship to ENSO in the NASA global coupled model and in observations. *J. Geophys Res.*, doi:10.1029/2007 JD009230.

Teng, Q., A.H. Monahan, and J.C. Fyfe, 2004: Effects of Time Averaging on Climate Regimes. *Geophys. Res. Lett.*, **31**, doi:10.1029/2004GL020840.

Wu, R. and S. Xie, 2003: On Equatorial Pacific Surface Wind Changes around 1977: NCEPNCAR Reanalysis versus COADS Observations. *J. Climate*, **16**, 167–173.

Wu, A. and W.W. Hsieh, 2002. Nonlinear canonical correlation analysis of the tropical Pacific wind stress and sea surface temperature. *Clim. Dyn.*, **19**, 713–722.

Zavala-Garay, J., A. Moore, C.L. Perez, and R. Kleeman, 2003: The response of a coupled model of ENSO to observed estimates of stochastic forcing. *J. Climate*, **16**, 2827–2842.

Zavala-Garay, J., C. Zhang, A. Moore, and R. Kleeman, 2005: On the linear response of ENSO to the Madden Julian Oscillation. *J. Climate*, **18**, 2441–2459.

Zhang, C., 2005: Madden-Julian Oscillation. *Rev. Geophys*, **43**, RG2003, doi:10.1029/2004RG000158.

Zhang, C. and J. Gottschalck, 2002: SST anomalies of ENSO and the Madden-Julian Oscillation in the equatorial Pacific. *J. Climate*, **15**, 2429–2445.

Zwiers, F.W. and H. von Storch, 1995: Taking serial correlation into account in tests of the mean. *J. Climate*, **8**, 336–351.